Journal of Alloys and Compounds 586 (2014) S498–S505

Contents lists available at SciVerse ScienceDirect

Journal of Alloys and Compounds

journal homepage: www.elsevier.com/locate/jalcom

Synthesis, characterization and high temperature CO_2 capture capacity of nanoscale Ca-based layered double hydroxides via reverse microemulsion

Po-Hsueh Chang [a], Yen-Po Chang [a], Yen-Ho Lai [a], San-Yuan Chen [a,*], Ching-Tsung Yu [b], Yau-Pin Chyou [b]

[a] Department of Materials Science and Engineering, National Chiao Tung University, Hsinchu 300, Taiwan
[b] Institute of Nuclear Energy Research, Taoyuan Country, Longtan 325, Taiwan

ARTICLE INFO

Article history:
Available online 7 June 2013

Keywords:
Coprecipitation
CO_2 absorption
Carbonation–calcination
Layered double hydroxide

ABSTRACT

In this study, we report a reverse microemulsion method to prepare stable homogeneous suspensions containing dispersed Ca–Al layered double hydroxide (LDH) nanoparticles. By changing the concentration, reaction time and temperature, the nano-particles with different structural morphology was developed from amorphous aggregation to platelet, regular hexagon and hydrangea-like hierarchical structure. The crystallization and growth of Ca–Al LDH nanoparticles were involved with a nucleation and growth process under nonaqueous polar solvent/surfactant system. After calcination at 700 °C, the calcined nano-sized Cal–Al LDH powders synthesized from the reverse microemulsion display remarkable CO_2 capture behavior at 600 °C, which is strongly dependent on the reaction conditions (concentration, time and temperature). The calcined powder synthesized at 80 °C exhibits a faster rate of CO_2 absorption and higher CO_2 capture capacity of 44 wt% CO_2 without apparent degradation under multiple cycles of carbonation–calcination.

1. Introduction

Over the past few years, there has been increasing demand for the capture of CO_2 due to the increasing awareness of the association between CO_2 accumulation in the atmosphere and global warming. Among the high-temperature (500–750 °C) solid CO_2 sorbents, layered double hydroxides (LDHs) [1-4], also known as hydrotalcite-like compounds or anionic clays, have been widely and intensively studied [5–10] because they possess both a high surface area and abundant basic sites at their surface, which are favorable for absorbing acidic CO_2. Among the various technologies and processes for synthesizing LDH powder, coprecipitation has been the most commonly adopted method to synthesize this material, in which the inorganic anions of nitrate, carbonate and chloride are used as interlayer counterions; however, the synthesized LDH powder usually forms large hexagonal platelets, which may affect its performance in many applications [11–14]. Therefore, it would be advantageous to develop an advanced materials fabrication process coupled with controlled particle morphology and size to enhance CO_2 capture capacity and reactivity. Among the techniques applied in the synthesis of ultrafine inorganic particles, reverse micelle, emulsion and microemulsion have been the most widely used techniques as microreactors for the controlled synthesis of oxides or binary oxides, such as Al_2O_3 [15], $ZnAl_2O_4$ [16], semiconductor nanoparticles [17,18], and metal nanoparticles [19].

Recently, several studies of M-Al LDHs (M = Mg, Ni, Co, etc.) using reverse microemulsion have been reported. Hu and O'Hare [20] controlled the synthesis of Mg–Al LDHs in a water-in-oil reverse microemulsion system to obtain nanometer-sized LDH platelets, which typically had a diameter of 40–50 nm and a thickness of 10 nm. Wang et al. [21] further investigated the growth and morphology of Co–Al LDH particles by adjusting the water-to-surfactant ratio. Up to now, for CO_2 sorbents used at high-temperatures (500–750 °C) [22,23], CaO-based materials have been best candidates because they have the largest capacity for CO_2 capture (approximately 0.7 mol/g-CaO). However, the CaO-based usually suffers from a major loss-in-capacity, i.e., a sharp decrease in CO_2 capture capacity with an increasing number of carbonation/calcination cycles [24]. To reduce the degradation of CO_2 capture, Martavaltzi and Lemonidou [22] prepared CaO–$Ca_{12}Al_{14}O_{33}$ sorbents using the calcium precursors of $Ca(OH)_2$ and $Ca(CH_3COO)_2$, and found that the $Ca_{12}Al_{14}O_{33}$ can inhibit the absorption capability of CO_2 sorbent over the much carbonation/calcination cycles. Recently, some researchers investigated a series of CaO-based sorbents derived from different calcium and aluminum precursors and obtained a high-performance CO_2 sorbent [25,26]. On the other hand, although Ca-based LDHs have been

* Corresponding author. Address: Department of Materials Science and Engineering, National Chiao Tung University, 1001 Ta-Hsueh Road, 300 Hsinchu, Taiwan. Tel.: +886 3 5731818; fax: +886 3 5724727.
E-mail address: sanyuanchen@mail.nctu.edu.tw (S.-Y. Chen).

0925-8388/$ - see front matter © 2013 Elsevier B.V. All rights reserved.
http://dx.doi.org/10.1016/j.jallcom.2013.05.213

considered to be promising candidates for capturing CO_2 due to their high reactivity with CO_2, little research has focused on the development of Ca-based LDHs nanoparticles using reverse microemulsion. During the CO_2 capture process, the crystalline phase, particle size and morphology of the CO_2 sorbents have played fairly important roles in the absorption kinetics and cycle performance. Therefore, in this study, we utilized reverse microemulsion to develop nano-scale Ca–Al LDHs within a limited space by controlling the supersaturated aqueous mixture of reactants in aqueous microreactors. To the best of our knowledge, no other previous work has been reported on the synthesis of Ca–Al LDHs in a water-in-oil system. The microemulsion-mediated synthesis at various concentration, reaction temperatures and time will be studied because the reaction parameters will affect the size and morphology of the isolated LDH crystallites. The morphology evolution of Ca–Al LDHs with reaction conditions was also investigated. Moreover, the CO_2 capture behavior of Ca–Al LDHs synthesized via reverse microemulsion is also discussed in this work.

2. Experimental details

2.1. Preparation of materials

Ca–Al–SDS LDHs with a Ca/Al molar ratio of 3 were synthesized using a reverse microemulsion process in which $Ca(NO_3)_2{\cdot}4H_2O$ (Sigma–Aldrich, 99%, US) and $Al(NO_3)_3{\cdot}9H_2O$ (Sigma–Aldrich, 99%, US) were dissolved in 30 mL of deionized water to make solution A (designated as LDH). Sodium dodecyl sulfate (SDS, Sigma–Aldrich, approximately 95%, US) and isooctane (100 mL, Sigma–Aldrich, 99%, US) were mixed in a 150 mL three-neck flask, and 1-butanol (Sigma–Aldrich, 99.4%, US) was added dropwise until the reverse microemulsions were stable and transparent. Then, 2 mL of solution A was added to the microemulsion and stirred until all reactants had dissolved at room temperature. Finally, 0.48 mol NaOH and 0.03 mol $NaNO_3$ were added to the mixture to adjust the pH to 10, and the reaction solution was treated at various temperatures, including 25, 80, 125 and 150 °C for different reaction time of 10 min, 1 h, 6 h, and 24 h, where each slurry was placed in a 200 mL stainless steel cell with a Teflon lining. To remove nitrate salts and unreacted SDS, the solids were subsequently refluxed and magnetically stirred in an ethanol/water mixture and then in acetone for 8 h. A white precipitate was formed and collected by high-speed centrifugation, washed with distilled water and acetone, and then dried at 80 °C in an oven to obtain raw LDH powder. In addition, for comparison, triple concentration precursor of $Ca(NO_3)_2{\cdot}4H_2O$ and $Al(NO_3)_3{\cdot}9H_2O$ was also used for synthesizing the Ca–Al–SDS LDHs particles following the above-mentioned similar procedure (designated as H-LDH) where the Ca/Al molar ratio of 3 is still maintained. The dried solid particles were crushed using a mortar and pestle and stored in a glass sample bottle for subsequent characterization.

2.2. Characterization of materials

Powder X-ray diffraction (PXRD) data were collected using an M18XHF theta–two theta diffractometer using Cu Kα radiation in a standard two-circle X-ray diffractometer operated at 50 kV and 200 mA. Diffraction data were recorded at two theta values between 1° and 50° to identify the existing crystalline phases based on comparison with the JCPDS diffraction data files. The particle morphologies of both the as-synthesized and calcined particles were examined using scanning electron microscopy (FE-SEM, JEOL-6700). Thermal gravimetric analysis (TGA, TA Instrument Q500) was used to investigate the CO_2 absorption properties of the calcined LDH samples (designated as nano-LDO) at 700 °C with a heating rate of 30 °C min^{-1}. The samples were maintained at high temperature for 20 min under nitrogen followed by CO_2 with a flow rate of 60 mL/min. Multiple carbonation–calcination cycles with the nano-LDO sorbents were performed at 600 °C for 10 min for carbonation in pure CO_2 gas and at 700 °C for 8 min for calcination in N_2 gas with flow rates of 60 mL/min to determine the thermal stability.

3. Results and discussion

3.1. Formation mechanism of Ca–Al–SDS LDH microspheres

A reverse microemulsion system was used to synthesize Ca–Al–SDS LDH nanoparticles in which the SDS anionic surfactants would be dissolved in organic solvents to form spheroidal reverse micelles within an isolated space. The normal SDS–water–isooctane system can provide separated spheroidal microemulsions as microreactors for the nucleation and crystallization of LDHs. In addition, the hydrophilic end with a negatively charged SDS ($CH_3(CH_2)_{11}OSO_3{-}Na^+$) can attract Ca^{2+} and Al^{3+} to enter the microemulsion.

Furthermore, the Ca^{2+} and Al^{3+} metal cations would react with OH^- ions to form Ca–Al LDH nuclei during the coalescence and decoalescence between water pools when the two systems are mixed together. The formation of Ca–Al LDH nanoparticles in reverse microemulsions is illustrated in Scheme 1. First, stable and transparent microemulsions were formed by mixing SDS, isooctane, and deionized water, followed by the dropwise addition of 1-butanol as a cosurfactant (Scheme 1a). Subsequently, Ca(NO3)2·4H2O, Al(NO3)3·9H2O and alkaline solution were dissolved in the microemulsion to initiate nucleation at pH ~6, after which the system became a translucent white color at pH 10. Following the in situ phase transformation of boehmite and the absorption of Ca^{2+} and NO_3^-, the Ca–Al LDH phase begins to crystallize, as illustrated in Scheme 1b. Upon heating at elevated temperatures from RT to 150 °C, crystal growth proceeded to form Ca–Al LDH nanocrystals with various morphologies (Scheme 1c). Finally, through reflux and drying steps, nano-scale Ca–Al–SDS LDH is formed (Scheme 1d). Therefore, SDS not only induced LDH formation in the nuclear space but also incorporated SO_4^{2-} anions for charge compensation in the interlayer spacing.

3.2. Characterization and properties of nano-scale Ca–Al LDH

To better understand the formation of Ca–Al–SDS LDH under different reaction time and temperatures within the microemulsion system, powder XRD patterns were obtained for SDS-intercalated Ca–Al LDH at different temperatures and aging times and are shown in Fig. 1: (a) 80 °C, 6 h (LDH-80-6); (b) RT, 24 h (LDH-RT-24); (c) 80 °C, 24 h (LDH-80-24); and (d) 150 °C, 24 h (LDH-150-24). Neither LDH-80-6 nor LDH-RT-24 exhibits a low angle Bragg reflection (003), most likely due to the short aging time and the low reaction temperature, respectively. In contrast, an intense peak in the very low angle Bragg reflection region can be observed for both LDH-80-24 (two theta = 2.63°, d_{003} = 33.6 Å) and LDH-150-24 (two theta = 2.65°, d_{003} = 33.3 Å), which indicates that for a high heating temperature or longer treatment time, a well-defined crystalline structure could be produced along the *c*-axis. These Bragg reflections are indexed as a (003) reflection of hexagonal unit cells with $c = 3d_{003}$ = 100.8 Å and 99.9 Å for LDH-80-24 and LDH-150-24, respectively. Moreover, the results from the Scherrer analysis appear to suggest that the crystallite size increases from 60 nm to 100 nm for LDH-80-24, LDH-125-24 and LDH-150-24 as the reaction temperature increases from 80 °C to 125 °C to 150 °C (Table 1). In addition, the $Ca(OH)_2$ phase was observed, which indicates that not all of the added Ca^{2+} ions can react with Al^{3+} to form SDS-intercalated Ca–Al LDH, as evidenced in Fig. 1. The formation of a $Ca(OH)_2$ phase, aside from the formation of a designed hydrotalcite (HT)-like phase, is presumably attributed to the greater insolubility of Ca in the LDH and to the incompatibility of the ionic sizes of Al and Ca (0.62 Å versus 1.06 Å). This result indicates that only a limited amount of Ca can be completely associated with the structural development into a stoichiometric Ca–Al LDH.

In addition, the samples with different concentration (LDH and H-LDH) were synthesized to study the effect of supersaturation concentration on the structural development of nano-scale Ca–Al–SDS LDHs at different reaction temperature for 24 h. As illustrated in Fig. 2a, the XRD patterns show that at RT, in addition to the formation of $Ca(OH)_2$ and $CaCO_3$, a higher concentration (H) does enhance the crystallization of Ca–Al–SDS LDH. As increasing treatment temperature such as 80 °C and 150 °C, the LDH peaks become strong and sharp, indicating a high treatment temperature can promote the growth and crystallization of Ca–Al–SDS LDH particles, as shown in Fig. 2d–f. Similar trend is also observed for the

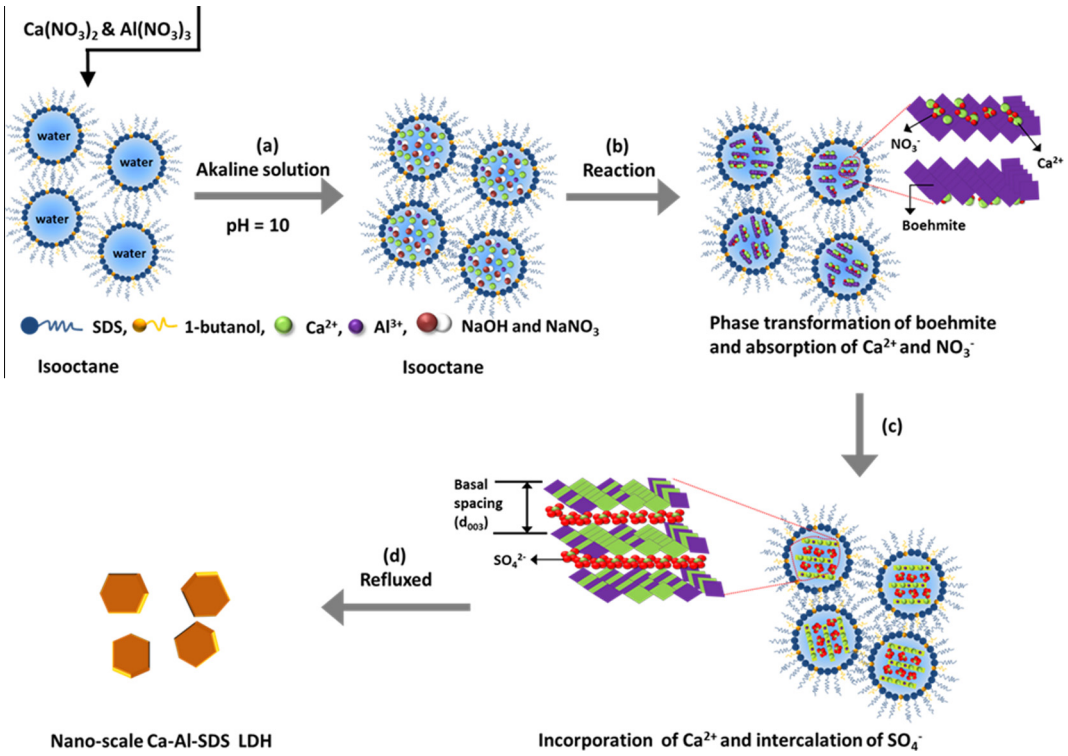

Scheme 1. Schematic illustration for the formation of Ca–Al LDH particles in reverse microemulsions: (a) stable and transparent microemulsion containing a mixture of metal salts, (b) in situ phase transformation of boehmite and absorption of Ca^{2+} and NO_3^-, (c) formation of crystal nuclei and crystallization of LDH, and (d) resulting nano-LDH.

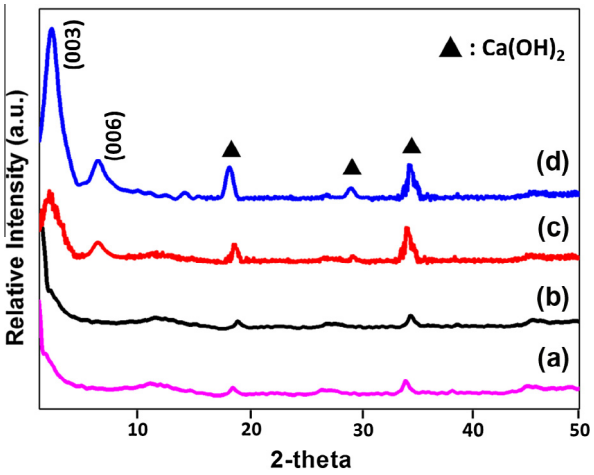

Fig. 1. XRD patterns of SDS-intercalated Ca–Al LDH at different temperatures and aging times (a) 80 °C, 6 h (LDH-80-6), (b) RT, 24 h (LDH-RT-24), (c) 80 °C, 24 h (LDH-80–24), and (d) 150 °C, 24 h (LDH-150-24).

other concentration as shown in Fig. 2a–c. However, it was also found that $CaCO_3$ phase was also formed for a higher concentration because more complex reactions can be initiated to form various phases. Furthermore, the effect of reaction time on the growth and crystallization of nano-LDH was also investigated. As shown in Fig. S1, the XRD of the nano-LDH treated at 80 °C for various time indicates that the high-concentration (H-LDH) displays a higher crystallization than low-concentration (LDH) at short time (6 h) and long time (24 h).

Thermogravimetric analysis (TG) of the thermal decomposition of the CO_2 sorbent is important for evaluating its feasibility. Fig. 3 shows the TG/DTG curves of the LDH-RT-24, LDH-80-24, LDH-125-24, and LDH-150-24 sorbents. Except for LDH-RT-24, the samples have similarly shaped curves with two distinct weight loss regions. First, there is an initial decrease in weight of approximately 15% in the temperature range of 30–230 °C, which is almost entirely due to the loss of loosely bound water at the surface and in the interlayer space [27]. Next, the weight loss appearing at 230–340 °C is attributed to the surfactant through the loss of the interlayer charge compensating anions and the dehydroxylation of hydrotalcite. The weight loss at ca. 440 °C is due to the degradation of the hydroxide in calcium hydroxide. The weight loss at ca. 670 °C corresponds to the degradation of the organic residue within the interlayer [28]. Furthermore, based on the DTG curves, the LDH-RT-24 sorbent exhibits the most complex reaction and slowest decomposition rate compared to the other LDH-80-24, LDH-125-24, and LDH-150-24 sorbents in the decomposition temperature range of 100–500 °C.

3.3. Morphology evolution

Previous studies have reported that, in a reverse microemulsion system, reaction parameters such as time, temperature, and solute addition must be considered when investigating the structural evolution. The particle size and morphology are highly dependent on both the heating time and temperature. Under these synthesis conditions, the aqueous phase that contains the ions required for growth of the Ca–Al LDH crystallites will be dispersed in the oil phase to form droplets surrounded by SDS groups under different reaction times and temperatures. Fig. 4 shows the morphology of the formed nanoparticles in the reverse microemulsions following thermal treatment at 80 °C for different periods of time (10 min, 1 h, 6 h, and 24 h). The nanoparticles synthesized in 10 min become quite irregular (Fig. 4a). As the treatment time increases to 1 h, the particles aggregate, and numerous tiny nanoparticles are

Table 1
Characterization of Ca–Al–SDS LDH samples.

Samples	d_{003} (Å)	D[a] (mn)	Ca (mole)	Al (mole)	The content of CaO (wt%)	Surface area[b] ($m^2\ g^{-1}$)		Pore volume ($cm^3\ g^{-1}$)	Average pore size[c] (nm)
						Raw LDH	Nano LDO (C700)		
LDH-RT-24	–nd	–nd	0.74	0.26	60.9	55.7	62.7	0.109	20.2
LDH-80-24	33.6	61	0.74	0.26	60.9	85.8	111.4	0.146	13.1
LDH-125-24	33.5	84	0.76	0.24	63.5	88.4	110.2	0.155	12.4
LDH-150-24	33.3	99	0.75	0.25	62.2	92.6	98.7	0.168	11.5

[nd] No detected.
[a] Crystallite size by Scherrer equation.
[b] BET surface area.
[c] BJH desorption average pore diameter.

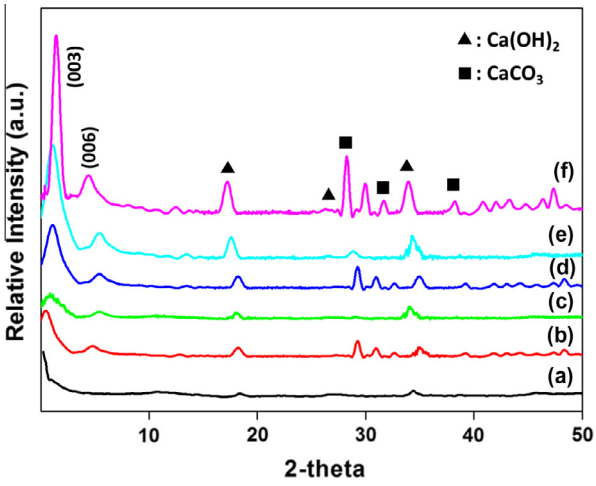

Fig. 2. XRD patterns of Ca–Al LDH from different supersaturation concentration at 24 h with different reaction temperatures (a) LDH-RT, (b) H-LDH-RT, (c) LDH-80 °C, (d) H-LDH-80 °C, (e) LDH-150 °C, and (f) H-LDH-150 °C.

distributed along the entire surface of the samples (Fig. 4b). These tiny nanoparticles would be the initial crystal nuclei at the early crystallization stages necessary for the later growth of crystalline Ca–Al LDH. The process is then thermodynamically driven further toward crystallization of these tiny nanoparticles with an increase in reaction time, and thus, irreversible aggregation of these randomly moving nanoparticles results in self-clustering growth to form platelet architectures (Fig. 4c). As thermal treatment continues at 24 h, Fig. 4d shows that the primary particle size doubles and that a regular hexagon structure stacks and forms due to the rearrangement of these LDH nanocrystallites, which is in good agreement with the XRD results (Fig. 1c) in which increasing reaction time can lead to enhanced crystallization and growth of the Ca–Al LDH phase.

To further understand the effect of the reaction temperature on the nucleation and growth of Ca–Al LDH, SEM micrographs were recorded. Fig. 5 shows the morphology evolution of Ca–Al LDH for 24 h under different heating temperatures at (a) RT, (b) 80 °C, (c) 125 °C, and (d) 150 °C. First, the SEM micrographs show agglomerates of amorphous gel particles and interconnected particles with heterogeneous shapes at room temperature (Fig. 5a). Then, at 80 °C, we found that particle disaggregation–reaggregation occurred and formed regular hexagonal Ca–Al LDH platelets, as shown in Fig. 5b. In this figure, the temperature-driven process appears to be the main event during the dissociation of amorphous LDH materials and the deposition processes for crystal growth to form LDH crystals with higher crystallinity.

Upon heating at elevated temperatures (125 °C and 150 °C), reactions such as disaggregation, particle growth, and reaggregation occur in series and/or in parallel. Nevertheless, the formation of M–OH bonds along the *a* and *b* axes is thermodynamically more favored than the layer stacking along the *c* axis via electrostatic interactions. Kinetically, the formation of M–OH bonds along the *a* and *b* axes involves a simpler and quicker precipitation process, whereas the layer stacking involves at least one additional coordinated absorption process of anions on the precursor hydroxide layers. Therefore, these high temperature driving forces would tend to induce oriented growth of the LDHs along the *a* and *b* axes, producing perpendicular plate-like LDH crystallites; however, the limited water-pool space would inhibit the growth of LDH plates, which then enables every possible precipitating species to precipitate, leading to a number of uniform nuclei (crystallites) that contain severe defects and that are interconnected by sharing edges and surfaces of sheet-like crystallites to form hydrangea-like LDH aggregates, as shown in Fig. 5c. At a sufficiently high temperature (150 °C), the hydrangea-like hierarchical structure was completely developed as a result of recrystallization of the sub-nanoparticles in the microspheres into thin sub-nanoplatelets, which are the most stable crystal form of Ca–Al LDHs (Fig. 5d).

For comparison, a high-concentration precursor was used to compare the effects of reaction temperature and time on structure development. The SEM images in *Fig.* S2 shows that the irregular particles were observed for the high-concentration solution treated at RT for 24 h, but a higher temperature, i.e., 150 °C, promotes the growth and stack of crystalline platelet along with some minor secondary particles on the platelets such as $CaCO_3$, which is consistent with the observation of XRD in Fig. 2. As extending the treatment time from 6 h to 24 h at 80 °C, although the growth and crystallization still can be enhanced for H-LDH and LDH, the $CaCO_3$ phase can be still observed on the H-LDH lamella (platelet) for a high-concentration solution, as shown in Fig. S3. The above-mentioned results again demonstrate that the synthesis temperature has a great influence on both the structure and morphology of the particles produced.

When these synthesized nanopowders were calcined at 700 °C, the hydrotalcite-like structure of Ca–Al LDH was completely destroyed, as shown in Fig. 6. The LDH-RT-24 sample in Fig. 6a displayed inhomogeneous aggregation due to the stacking of small particles and large lumps. However, no strong agglomeration phenomena occurred in the samples synthesized at higher heating temperatures (80 °C, 125 °C and 150 °C), as evidenced in Fig. 6b–d, revealing well-dispersed calcined nanoparticles (~40 nm) that were likely correlated with the hierarchical LDH structure evolved from the reverse microemulsion reaction at 80–150 °C, which is quite consistent with the XRD patterns in Fig. 1. When calcined at 700 °C, additional Ca–Al LDH layers in the hierarchical structure would be exfoliated and transformed into separated individual nanoplatelets, leading to homogeneous nano-scale Ca–Al–O mixed oxides. Here, it was also observed that the calcined Ca–Al–O nanoparticles synthesized at 150 °C possess a slightly larger size compared to those synthesized at 80 °C and 125 °C.

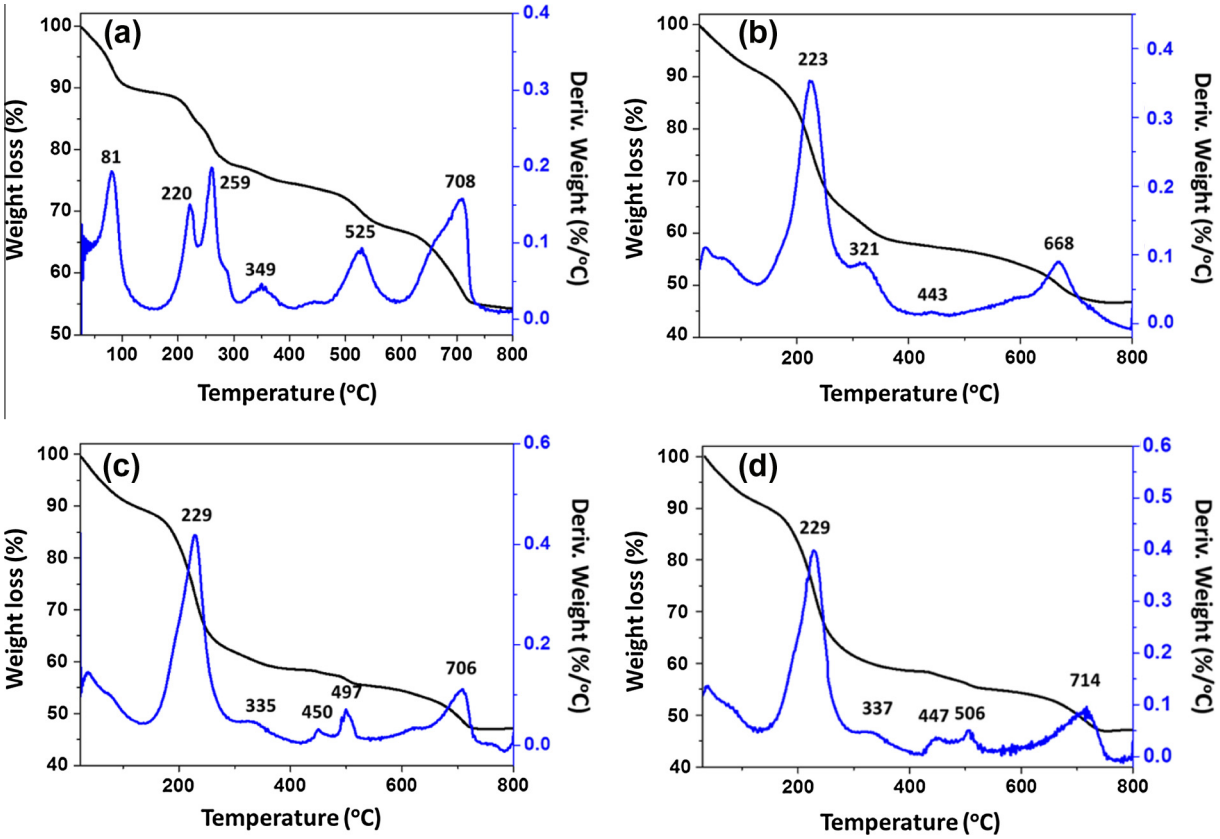

Fig. 3. TG and DTG curves of LDH-RT-24, LDH-80-24, LDH-125-24, and LDH-150-24.

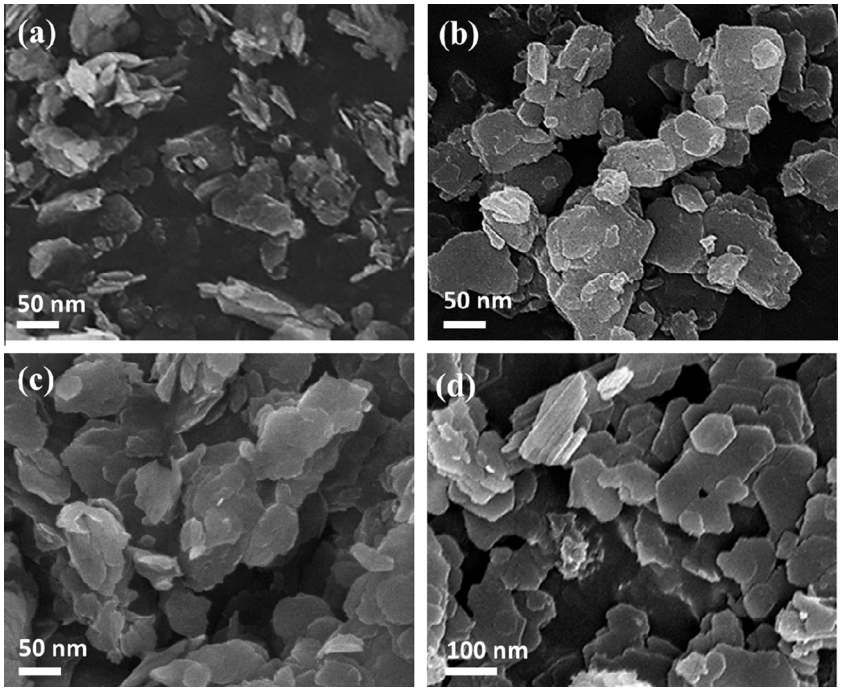

Fig. 4. FE-SEM micrographs of the particle morphology grown in a reverse microemulsion at 80 °C for (a) 10 min, (b) 1 h (c) 6 h, and (d) 24 h.

Fig. 7 shows the XRD patterns of nano-LDO powders calcined at 700 °C as a function of the heating temperature. It was found that only the CaO phase was detected in the LDH-RT-24 sample. However, by increasing the heating temperature, a secondary phase of calcium aluminum oxide ($Ca_{12}Al_{14}O_{33}$) formed, thus indicating that the formation of $Ca_{12}Al_{14}O_{33}$ can be promoted during calcination due to the close contact of Ca–Al in the Ca–Al LDH structure.

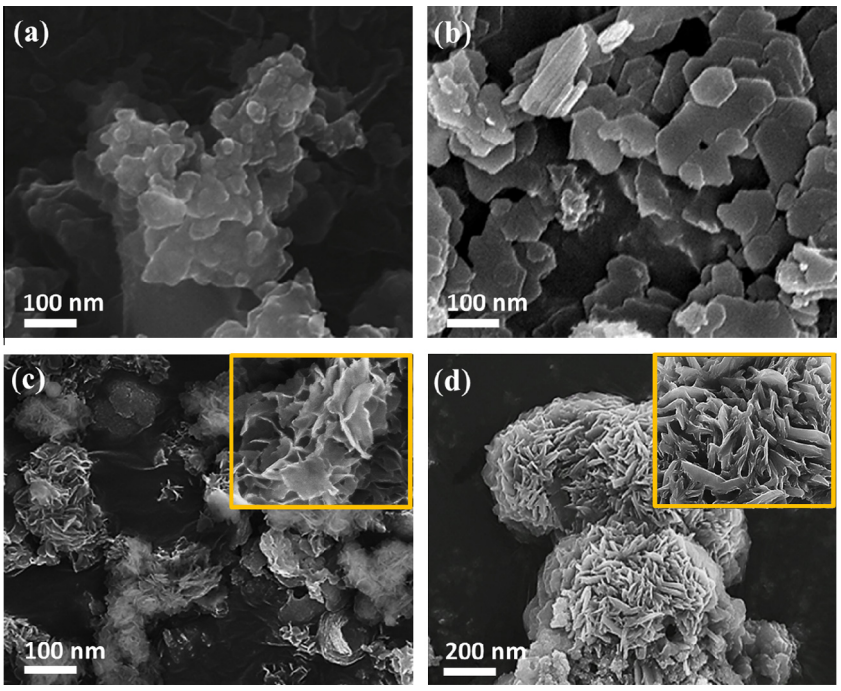

Fig. 5. FE-SEM micrographs of nanoparticles synthesized from reverse microemulsion at 24 h with a reaction temperature of (a) RT, (b) 80 °C, (c) 125 °C, and (d) 150 °C.

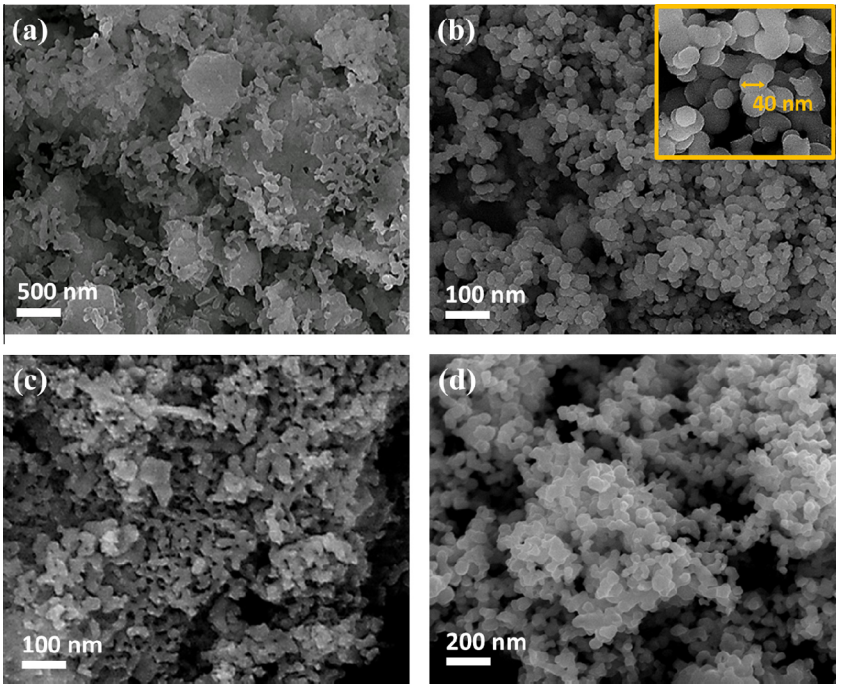

Fig. 6. FE-SEM micrographs of the 700 °C-calcined nanopowders as a function of different heating temperatures: (a) RT, (b) 80 °C, (c) 125 °C, and (d) 150 °C at 24 h.

3.4. CO_2 capture behavior

Fig. 8a shows the CO_2 absorption curves of the nano-LDO with a 3:1 Ca/Al ratio at 700 °C as a function of heating temperature ranging from RT to 150 °C. A maximum capture capacity of 44 wt% occurred in samples heating treated at RT and 80 °C. When the heating temperature increased from RT to 150 °C, the CO_2 capture capacity decreased from 44, 43, 35, to 33 wt%, for which two reaction stages can be clearly identified for all the absorptions: the fast reaction at the initial stage of CO_2 absorption over a relatively short time period, approximately 4–10 min, can be explained by control of the chemical reaction, whereas at a later time periods, a continuous but much slower increase in sample weight was observed, which is controlled by diffusion. Moreover, it is found that, except for the RT-treated sample, the heat-treated nano-LDO samples exhibit a more rapid CO_2 absorption rate. Furthermore, Table 1 shows

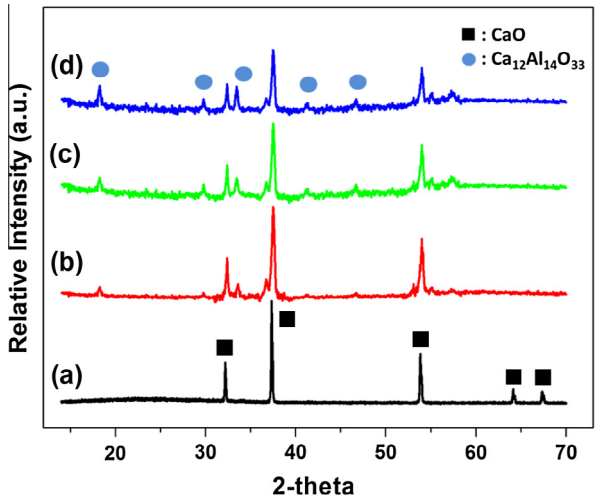

Fig. 7. XRD patterns of 700 °C-calcined Ca–Al LDH powders as a function of different heating temperatures: (a) RT, (b) 80 °C, (c) 125 °C, and (d) 150 °C at 24 h.

that the BET surface area of the LDH-80-24 sample calcined at 700 °C possessed the highest total surface area (111.4 $m^2 g^{-1}$ compared to 62.7 $m^2 g^{-1}$ for the LDH-RT-24 sample), indicating that a very open structure with a larger total pore volume was obtained and is the main reason for the absorption rate of the LDH-80-24 sample.

Fig. 8b shows the CO_2 capture capacity of four nano-LDO sorbents (RT, 80 °C, 125 °C and 150 °C) as a function of the carbonation–calcination cycle number of sorbents performed at 600 °C for 10 min for carbonation in pure CO_2 gas and at 700 °C for 8 min for calcination in N_2 gas for 40 cycles. The CO_2 capture capacity of the LDO-RT-24 sorbent decreases from 40.3 wt% to 27.1 wt% over 40 cycles. In contrast, although the maximum capture capacity of the LDO-150-24 sorbent was approximately 33 wt%, which is smaller than that of the LDO-RT-24 sorbent, a CO_2 capture capacity as high as 95% of the first-cycle CO_2 capture capacity was maintained over 40 carbonation–calcination cycles, i.e., there was a decrease of only 5%, which corresponds to a 0.13 wt% reduction on average per cycle. The carbonation process is strongly related to the formation of calcium aluminum oxide ($Ca_{12}Al_{14}O_{33}$) because $Ca_{12}Al_{14}O_{33}$ can inhibit the aggregation and partial sintering between CaO/$CaCO_3$ particles, but it does not function like CaO to capture CO_2. In comparison, the LDO-80-24 sorbent not only possessed a much greater CO_2 capture capacity of 43 wt% but also maintained that CO_2 capture capacity over multiple cycles without apparent reduction, suffering only minimal degradation (as compared to bulk CaO in Fig. S4). This phenomenon can be attributed to the formation of a small amount of nano-scale calcium aluminum oxide $Ca_{12}Al_{14}O_{33}$ that enhances the CO_2 capture performance, as evidenced in the XRD patterns in Fig. 6. The above results clearly demonstrate that the sorbents developed from reverse microemulsion possess a significantly faster rate of CO_2 absorption and greater CO_2 capture capacity without apparent degradation. In addition, it was found that the maximum absorption capacity of the calcined LDH particles developed from a high-concentration solution via increasing its reaction temperature or time was obviously decreased as compared to that from low-concentration solution, as shown in Fig. S5. This is can be attributed to the fact that large platelets and minor $CaCO_3$ phase will lead to the reduction in CO_2 absorption capacity of the calcined LDH particles.

4. Conclusion

In summary, the nano-scale Ca–Al–SDS LDHs can be synthesized within the limited space available using a reverse microemulsion. The structural morphology and crystallization of Ca–Al–SDS LDHs can be modified by controlling the concentration, heating temperature and time. By increasing the solution concentration, reaction temperature and time, the growth and crystallization of nano-scale Ca–Al–SDS LDHs can be promoted but some minor phases such as $CaCO_3$ were easily formed in a high-concentration solution because of the enhanced reaction kinetics. On the other hand, a low temperature treatment is not beneficial to the crystallization process. Therefore, this study demonstrates that the nano-LDH-80-24 displays optimal LDH structure and morphology and the corresponding calcined nano Ca–Al LDO powders possess a high CO_2 absorption capacity. In addition, the high CO_2 capture capacity of the sorbents could largely be maintained over multiple cycles of utilization because the Al^{+3} cations are well incorporated into the calcium oxide nanoparticles to form $Ca_{12}Al_{14}O_{33}$ oxide which can avoid the intimate contact between CaO nanoparticles. In particular, this developed calcined nano Ca–Al LDO has excellent thermal stability and regeneration capacity in cyclic use, which is one of the key factors required for several carbonation applications.

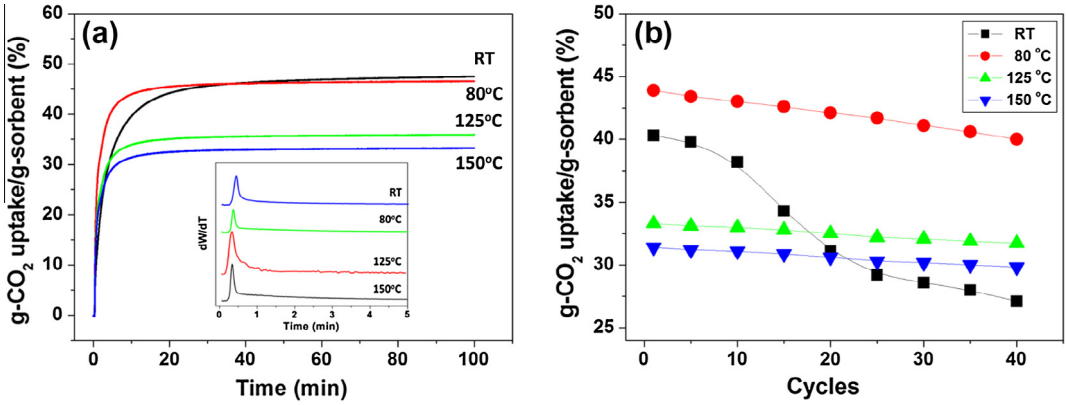

Fig. 8. (a) CO_2 absorption kinetics of calcined nano-Ca/Al LDH (calcined at 700 °C) for different heating temperatures and (b) multiple cycles of carbonation–calcination for calcined nano-Ca/Al LDH (C700) in 100% CO_2 for 10 min (carbonation) at 600 °C and in 100% N_2 for 8 min (calcination) at 700 °C.

Acknowledgments

This work was financially supported by the authors gratefully acknowledge the financial support of the National Science Council of Taiwan through Contract No. 102-3113-P-042A-005 and Institute of Nuclear Energy Research.

Appendix A. Supplementary material

Supplementary data associated with this article can be found, in the online version, at http://dx.doi.org/10.1016/j.jallcom.2013.05.213.

References

[1] Z. Yong, A.E. Rodrigues, Energy Convers. Manage. 43 (2002) 1865–1876.
[2] J.W. Boclair, P.S. Braterman, B.D. Brister, Z.M. Wang, F. Yarberry, J. Solid State Chem. 161 (2001) 249–258.
[3] D.R. Hines, S.A. Solin, Phys. Rev. B. 61 (2000) 11348–11358.
[4] Seida et al., J. Chem. Eng. Jpn. 34 (2001) 906.
[5] M.K. Ram Reddy, Z.P. Xu, G.Q. (Max) Lu, J.C. Diniz da Costa, Ind. Eng. Chem. Res. 45 (2006) 7504–7509.
[6] Léa Desigaux, Malha Ben Belkacem, Peggy Richard, Joe Cellier, Philippe Léone, Laurent Cario, Fabrice Leroux, Christine Taviot-Guého, Bruno Pitard, Nano Lett. 6 (2) (2006) 199.
[7] Stefanie Kuhl, Matthias Friedrich, Marc Armbr uster, Malte Behrens, J. Mater. Chem. 22 (2012) 9632–9638.
[8] Naveed Ahmed, Motoharu Morikawa, Yasuo Izumi, Catal. Today 185 (2012) 263–269.
[9] Irene Carpani, Mario Berrettoni, Marco Giorgetti, Domenica Tonelli, J. Phys. Chem. B 110 (2006) 7265–7269.
[10] Irene Carpani, Marco Giorgetti, Mario Berrettoni, Pier Luigi Buldini, Massimo Gazzano, Domenica Tonelli, J. Solid State Chem. 179 (2006) 3981–3988.
[11] X. Xu, R. Lu, X. Zhao, S. Xu, X. Lei, F. Zhang, D.G. Evans, Appl. Catal. B: Environ. 102 (2011) 147.
[12] A.C.S. Alcantara, P. Aranda, M. Darder, E.J. Ruiz-Hitzky, Mater. Chem. 20 (2010) 9495.
[13] A.J. Vizcaíno*, M. Lindo, A. Carrero, J.A. Calles, Int. J. Hydr. Energy 37 (2012) 1985–1992.
[14] A.F. Cunha, Y.-J. Wu, J.C. Santos, A.E. Rodrigues, Chem. Eng. Res. Des. 9 (1) (2013) 581–592.
[15] Y. Pang, X. Bao, J. Mater. Chem. 12 (2002) 3699.
[16] A.E. Giannakas, T.C. Vaimakis, A.K. Ladavos, P.N. Trikalitis, P.J. Pomonis, J. Colloid Interface Sci. 259 (2003) 244.
[17] M.L. Curria, A. Agostiano, F. Mavellib, M. Della Monica, Mater. Sci. Eng. C 22 (2002) 423.
[18] J. Xu, Y. Li, J. Colloid Interface Sci. 259 (2003) 275.
[19] X. Zhang, K. Chan, Chem. Mater. 15 (2003) 451.
[20] Hu Gang, Dermot O'Hare, J. Am. Chem. Soc. 127 (2005) 17808.
[21] Chengle J. Wang, Yimin A. Wu, Robert M.J. Jacobs, Jamie H. Warner, Gareth R. Williams, Dermot O'Hare, Chem. Mater. 23 (2011) 1710.
[22] C.S. Martavaltzi, A.A. Lemonidou, Ind. Eng. Chem. Res. 47 (2008) 9537.
[23] Rainer Filitz, Agnieszka M. Kierzkowska, Marcin Broda, Christoph R. Muiler, Environ. Sci. Technol. 46 (2012) 559.
[24] J.C. Abanades, D. Alvarez, Energy Fuels 17 (2003) 308–315.
[25] W.Q. Liu, B. Feng, Y.Q. Wu, G.X. Wang, J. Barry, J.C. Diniz Da Costa, Environ. Sci. Technol. 44 (2010) 3093–3097.
[26] Z.M. Zhou, Y. Qi, M.M. Xie, Z.M. Cheng, W.K. Yuan, Chem. Eng. Sci. 74 (2012) 172.
[27] N.D. Hutson, S.A. Speakman, E.A. Payzant, Chem. Mater. 16 (2004) 4135–4143.
[28] J. Zhu, P. Yuan, H. He, R. Frost, Q. Tao, W. Shen, T. Bostrom, J. Colloid Interface Sci. 319 (2008) 498–504.